

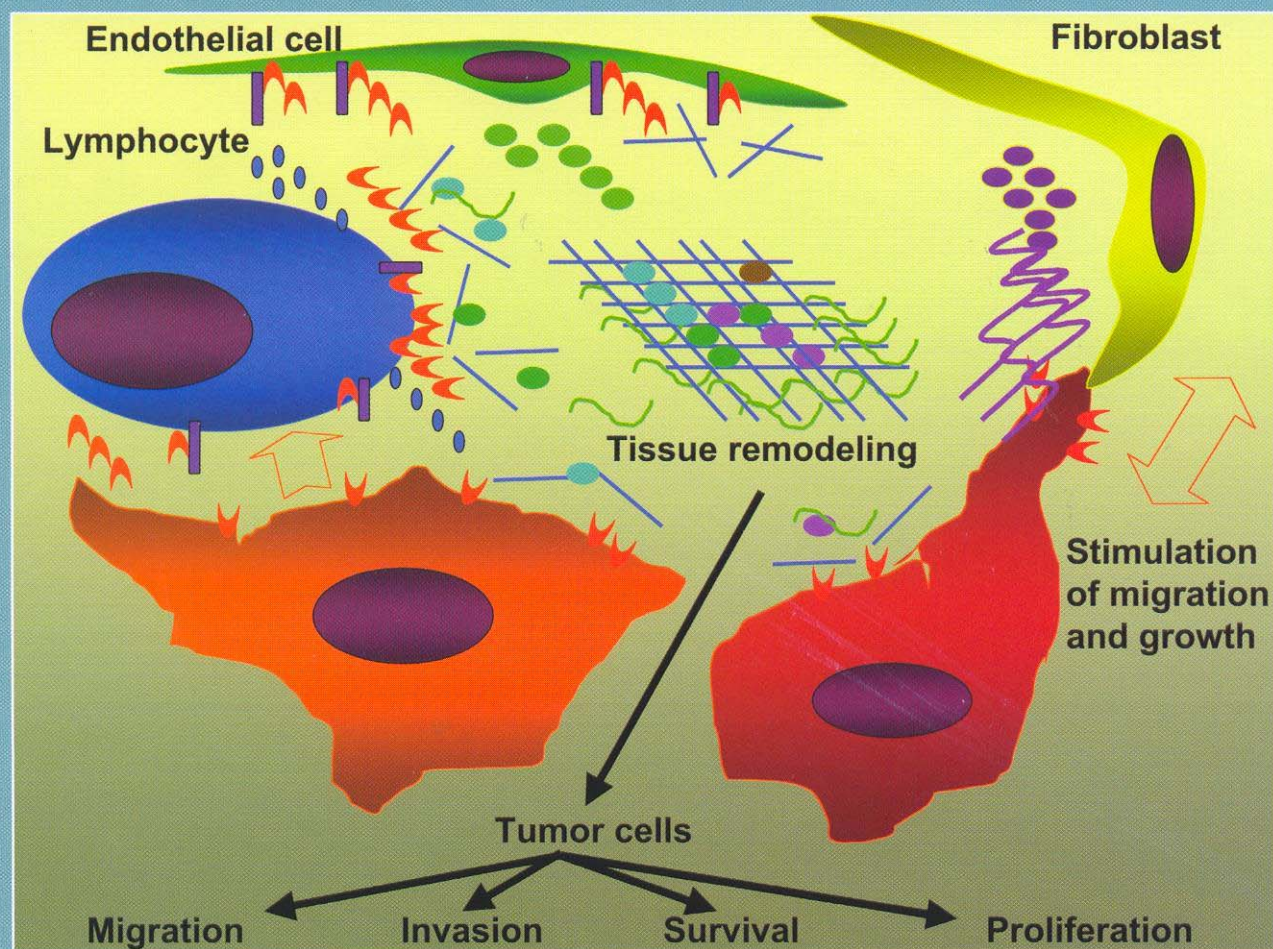
CANCER GROWTH AND PROGRESSION

Series Editor: Hans E. Kaiser

Integration/Interaction of Oncologic Growth

Edited by

Gary G. Meadows



Chapter 3

Imaging of Angiogenesis In Vivo with Fluorescent Proteins

Robert M. Hoffman

AntiCancer, Inc., 7917 Ostrow St., San Diego, CA 92111, USA

Abstract: We have adapted the surgical orthotopic implantation (SOI) model to image angiogenesis of human tumors labeled with green fluorescent protein (GFP) in nude mice. The nonluminous induced capillaries are clearly visible against the very bright tumor fluorescence examined either intravitaly or by whole-body imaging in real time. The fluorescence shadowing replaces the laborious histological techniques for determining blood vessel density. Intravital images of an SOI model of human pancreatic tumors expressing GFP visualized angiogenic capillaries at both primary and metastatic sites. Whole-body optical imaging showed that blood vessel density increased linearly over a 20-week period in an SOI model of human breast cancer expressing GFP. Opening a reversible skin-flap in the light path markedly reduces signal attenuation, increasing detection sensitivity many-fold. The observable depth of tissue is thereby greatly increased. With dual-color fluorescence imaging, effected by using red fluorescent protein (RFP)-expressing tumors growing in GFP-expressing transgenic mice that express GFP in all cells, great clarity the details of the tumor-stroma interaction, especially tumor-induced angiogenesis are visualized. The GFP-expressing tumor vasculature, both nascent and mature, are readily distinguished interacting with the RFP-expressing tumor cells. Using a spectral imaging system based on liquid crystal tunable filters, we were able to separate individual spectral species on a pixel-by-pixel basis. Such techniques non-invasively visualized the presence of host GFP-expressing vessels within the RFP-labeled tumor by whole-body imaging. This new differential dual-colored fluorescence imaging tumor-host model, along with spectral unmixing, can non-invasively visualize in real-time the onset and progression of angiogenesis in a tumor. Thus, fluorescent proteins expressed *in vivo* offer the highest resolution and sensitivity for real-time whole-body imaging of angiogenesis.

Key words: Green fluorescent protein, red fluorescent protein, imaging, mouse models

1. INTRODUCTION

1.1 Formation and Nature of Blood Vessels

Vasculogenesis is the formation of new blood vessels by endothelial progenitors. Angiogenesis is the sprouting and growth of existing vessels. Capillaries distribute the blood flow while proximal arterioles provide the bulk flow to tissue. Capillaries

consist only of endothelial cells (ECs), whereas larger vessels are surrounded by mural cells such as pericytes and smooth muscle cells (1). ECs differentiate from angioblasts in the embryo as well as from endothelial progenitor cells (EPCs) in the adult bone marrow. Vascular endothelial growth factor (VEGF), angiopoietin (Ang)-1, cytokines, and other signals stimulate vasculogenesis and angiogenesis (1).

1.2 Tumor Blood Vessels

Vessel walls are abnormal in tumors and have uneven diameters. ECs form an imperfect and uneven vessel lining, with wide junctions at some locations and stacked layers of ECs at others. Some ECs do not express endothelial markers such as CD31. ECs in tumors can undergo apoptosis, allowing cancer cells into the lumen resulting in mosaic vessels. Heterogeneity of tumor vessels is very common (2). Tumor vessels do not have the hierarchical branching pattern of normal vascular networks, resulting in avascular, hypoxic areas in the tumor (2). The abnormal organization and ultrastructure of tumor vessels makes the blood flow in tumor vessels chaotic and the vessels leaky (2). Due to remodeling of the vasculature, blood flow varies between a tumor and its metastases as well as within a given tumor from one location to another (2). A relative deficiency of pericytes, or pericyte function, could be responsible for the morphological features of tumor vasculature including their tortuous pattern (3).

Cancer cells may be part of vessel-like structures found within some tumors. This concept is known as 'vasculogenic mimicry' (4). Melanomas often have a histological pattern that is characterized by a network of periodic acid-schiff (PAS)-positive structures that appear to be channels formed without endothelial cells, which is different from cancer cells in the walls of blood vessels. Cancer cells have been reported to make up as much as 25% of the luminal surface of some tumor vessels, the remaining surface which is covered by an endothelium. The tumor cells in the vessel lining might be in transit, entering or exiting the vessel (3).

1.3 Methods of Imaging Blood Vessels (5)

Magnetic resonance imaging and computed tomography have resolutions of 100 to 500 μm . PET and ultrasonography have resolutions of a few millimeters. X-ray images, has a resolution of ~ 100 μm . Computed tomographic angiography and magnetic resonance imaging angiography require intravascular contrast agents, and resolution is insufficient to resolve microvasculature. Macromolecular magnetic resonance imaging

contrast agents enable resolution approaching 200 μm in animals and thus most angiogenic blood vessels are not resolved. Micromagnetic resonance imaging has a resolution of approximately 10 μm (5). Fluorescence has a resolution of approximately 100 nm (5) and therefore seems best suited for imaging blood vessels.

1.4 Models to Visualize Angiogenesis

Tumor angiogenesis is a critical step in tumor growth, progression, and metastasis. As such, angiogenesis promises a uniquely effective yet remarkably benign target for cancer chemotherapy. A major requirement for the effective discovery of angiogenesis-related drugs is an assay system that is accurate, rapid, and economical. We have developed model systems that meet these requirements (6).

The discovery and evaluation of antiangiogenic substances initially relied on *in vivo* methods such as the chorioallantoic membrane assay (7, 8), the monkey iris neovascularization model (9), the disk angiogenesis assay (10), and various models that use the cornea to assess blood vessel growth (11-16). Although they are important for understanding the mechanisms of blood vessel induction, these models did not deal with tumor angiogenesis and are poorly suited to drug discovery.

Subcutaneous tumor xenograft angiogenesis models have been developed to study tumor angiogenesis, but these require cumbersome pathological examination procedures such as histology and immunohistochemistry. Measurements require animal sacrifice and therefore preclude ongoing angiogenesis studies in individual, live, tumor-bearing animals. Moreover, xenografts are not representative models of human disease.

Tumors transplanted in the cornea of the rodents (17-19) and rodent skin-fold window chambers have also been used for angiogenesis studies (20-26). The cornea and skin-fold chamber models provide a means for studying angiogenesis in living animals. However, quantification requires specialized procedures, and the sites do not represent natural environments for tumor growth. The cornea and skin-fold window chamber tumor models do not allow orthotopic and metastatic angiogenesis, which

may involve mechanisms of angiogenesis (27) that are qualitatively different from these ectopic models.

1.5 Orthotopic Tumor Models Expressing GFP to Visualize Tumor Angiogenesis

A suitable model for drug discovery will accurately represent clinical cancer as well as enable real-time visualization of the angiogenesis process and its inhibition by effective agents. To develop realistic and real-time tumor angiogenesis models, we have used surgical orthotopic implantation (SOI) metastatic models of human cancer (28). These models place tumors in natural microenvironments and replicate clinical tumor behavior more closely than do ectopic implantation models (28). For these studies the tumors implanted in the orthotopic model have been transduced and selected to strongly express green fluorescent protein (GFP) *in vivo* (28).

GFP expression in primary tumors and in their metastases in the mouse models can be detected by an intense fluorescence seen by intravital or by whole-body imaging. The nonluminescent angiogenic blood vessels appear as sharply defined dark networks against this bright background. The high image resolution permits quantitative measurements of total vessel length. These genetically fluorescent tumor models thereby allow quantitative optical imaging of angiogenesis *in vivo*. Tumor growth, vascularization, and metastasis can now be followed in real time (28).

1.6 Intravital Images of Angiogenesis of Orthotopic Pancreas Cancer

The clarity of angiogenic blood vessel imaging was illustrated by intravital examination of the orthotopic growth of a Bx-PC-3-GFP pancreatic tumor. The nonluminescent blood vessels were clearly visible against the GFP fluorescence of the primary tumor. Angiogenesis associated with metastatic growths was also easily imaged by intravital examination (28).

1.7 Intravital Imaging of Angiogenesis of Orthotopic Prostate Cancer

Because angiogenesis could be measured without animal sacrifice, it was possible to determine a time course for individual animals. Sequential intravital images of angiogenesis for the human prostate tumor PC-3-GFP growing orthotopically in a single nude mouse were acquired. The tumor-associated blood vessels were clearly visible by day 7 and continued to increase at least until day 20 (28).

1.8 Whole-Body Imaging of Angiogenesis in Orthotopic Breast Cancer

We have demonstrated whole-body images and quantitation of the time course of angiogenesis of the MDA-MB-435-GFP human breast cancer growing orthotopically in the breast fat pad in a nude mouse. The development of the tumor and its angiogenesis could be imaged in a completely noninvasive manner (28). The mouse breast fat pad is the orthotopic environment for the implanted MDA-MB-435-GFP breast cancer and allows noninvasive, whole-body imaging of tumor angiogenesis. The quantitative angiogenesis data show that microvessel density increased over 20 weeks. Thus, tumors, even in their natural microenvironment, growing orthotopically in sites such as the fatpad and presumably others, can be whole-body imaged for quantitative angiogenesis studies (28).

1.9 Comparative Advantages of Fluorescent Tumor Imaging

Subcutaneous implantation sites (29-32) are not normal sites for tumor growth, and their microenvironments are very different from orthotopic sites with regard to regulation not only of tumor growth but of the angiogenesis process itself (27). Orthotopically implanted GFP-labeled tumors also allow the study of angiogenesis for metastasis. The orthotopically growing tumors, in contrast to most other models, give rise to spontaneous metastases that resemble, both in target tissues and in frequency of occurrence, the clinical behavior of

the original human tumor (33). Moreover, the extreme detection sensitivity afforded by the strong GFP fluorescence allows imaging of very early events in blood vessel induction. As Li *et al.* (24) point out, angiogenesis initiation in metastatic tumors may be very different from that of primary tumors and require different interventions.

1.10 Skin Flaps Enable Ultra-High Resolution External Imaging of Angiogenesis

Opening a reversible skin-flap in the light path markedly reduced signal attenuation, increasing detection sensitivity many-fold. The observable depth of tissue is thereby greatly increased (34). The brilliance of the tumor GFP fluorescence, facilitated by the reduced absorption through the skin-flap window, allowed imaging of the induced microvessels as dark against a bright background. The orthotopically growing BxPC 3-GFP human pancreatic tumor was visualized surrounded by its microvessels visible by their dark shadows (34).

1.11 Dual Color Tumor-Host Models

Okabe *et al.* (35) produced transgenic mice with GFP under the control of a chicken beta-actin promoter and cytomegalovirus enhancer. All of the tissues from these transgenic mice, with the exception of erythrocytes and hair, fluoresce green.

Tumor cells to be transplanted in the GFP mouse were made visible by transforming them with the red fluorescent protein (RFP) (28). In order to gain further insight into tumor-host interaction in the living state, including tumor angiogenesis, we have visualized RFP-expressing tumors transplanted in the GFP-expressing transgenic mice under dual-color fluorescence microscopy. The dual-color fluorescence made it possible to visualize the tumor growth in the host by whole-body imaging as well as to visibly distinguish interacting tumor and host cells in fresh tissue. The dual-color approach affords a powerful means of both visualizing and distinguishing the components of the host-tumor interaction (36).

1.12 Visualizing Angiogenesis Onset and Development by Dual-Color Imaging

Dual-color images of early events in tumor angiogenesis induced by a B16F10 mouse melanoma in the transgenic GFP expressing mouse were acquired in fresh tissue preparations. Host-derived GFP-expressing fibroblast cells and endothelial cells form nascent blood vessels were visualized clearly against the red fluorescent background of the RFP-expressing mouse melanoma. Host-derived GFP-expressing blood vessels within the RFP-expressing mouse melanoma became visible. The images were acquired three weeks after subcutaneous injection of B16F10-RFP melanoma cells in the GFP mouse.

1.13 Dual-Color Imaging with Spectral Resolution with Ultra-High Resolution Whole-Body Imaging of Angiogenesis

The MDA-MB-435 human breast tumor expressing RFP was orthotopically transplanted to the transgenic GFP nude mice. The RFP tumors growing in the GFP-mice were visualized using excitation centered at 470 nm and appropriate >500-nm emission filters. Using a spectral imaging system based on liquid crystal tunable filters, we were able to perform whole-body imaging yielding high-resolution spectral information at each pixel of the resulting image. Powerful analysis algorithms allow the separation (unmixing) of individual spectral species on a pixel-by-pixel basis. Such techniques non-invasively visualized the presence of host GFP-expressing stroma within the RFP-labeled tumor. Moreover, fluorescence spectra emitted in the far-red, allow the whole-body imaging of tumor angiogenesis. This new differential dual-colored fluorescence imaging tumor-host model, along with spectral unmixing, can non-invasively visualize in real-time the onset and progression of angiogenesis in a tumor. Other host cells and structures in the tumor may also be visualized by whole-body spectral imaging (37).

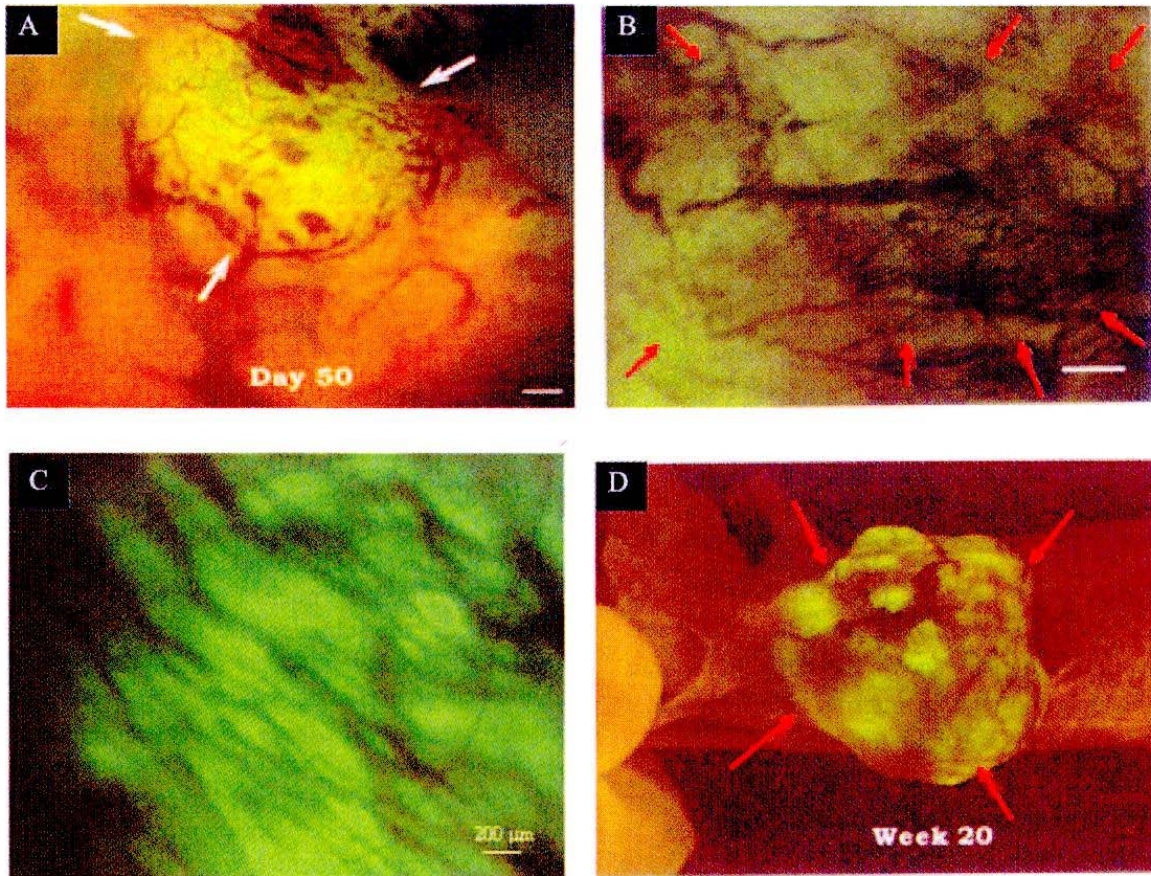


Figure 1. A. Intra vital fluorescence imaging of Bx PC 3 GFP human pancreas cancer angiogenesis in an orthotopic tumor. The GFP expressing human tumor was transplanted to nude mice by surgical orthotopic implantation (SOI) and intravitaly imaged 50 days later. Bar = 200 μm . *B.* Intra vital fluorescence imaging of PC 3 human prostate cancer angiogenesis in orthotopic primary tumor. The GFP expressing human tumor was transplanted to nude mice by SOI and imaged at day 19. Bar = 470 μm . *C.* Direct view of microvessels of orthotopically-growing pancreatic cancer. The human Bx PC-3-GFP pancreatic tumor, microvessels were directly viewed on day-58 after SOI and highly resolved through the skin flap window at higher magnification. Bar = 200 μm . *D.* Whole body fluorescence imaging of MDA MB 435 human breast cancer angiogenesis in orthotopic primary tumor. The GFP expressing human tumor was transplanted by SOI in the fat pad of nude mice and whole body imaged at week 20.

2. MATERIALS AND METHODS

2.1 Fluorescence Optical Imaging (6)

A Leica fluorescence stereo microscope model LZ12 equipped with a mercury lamp and a 50-W power supply was used. Selective excitation of GFP was produced through a D425y60 band-pass filter and a 470 DCXR dichroic mirror. Emitted

fluorescence was collected through a long-pass filter (GG475; Chroma Technology, Brattleboro, VT) on a Hamamatsu C5810 3-chip cooled color charge-coupled device camera (Hamamatsu Photonics, Bridgewater, NJ). Images were processed for contrast and brightness and analyzed with the use of IMAGE PRO PLUS 3.1 software (Media Cybernetics, Silver Spring, MD). High-resolution images of 1024 \times 724 pixels were captured directly on an IBM PC or continuously through video output

on a high-resolution Sony VCR (model SLVR1000; Sony, Tokyo).

2.2 Expression Vectors (38)

The pLNCX₂ vectors were purchased from Clontech Laboratories (Palo Alto, CA). The pLNCX₂ vector contains the neomycin resistance gene for antibiotic selection in eukaryotic cells. The RFP gene (DsRed2; Clontech Laboratories) was inserted in the pLNCX₂ vector at the Egl II and Not I sites.

2.3 GFP and RFP Vector Production (6, 36)

GFP expression vector. The pLEIN retroviral vector (CLONTECH) expressing enhanced GFP and the neomycin resistance gene on the same bicistronic message, which contains an internal ribosome entry site (6), was used to transduce tumor cells.

RFP expression vector. PT67, a NIH 3T3-derived packaging cell line expressing the 10 A1 viral envelope, was purchased from CLONTECH. PT67 cells were cultured in DMEM (Irvine Scientific) supplemented with 10% heat-inactivated FBS (Gemini Biological Products, Calabasas, CA). For vector production, packaging cells (PT67), at 70% confluence, were incubated with a precipitated mixture of *N*-[1-(2,3-dioleoyloxy)propyl]-*N,N,N*-trimethylammonium methylsulfate reagent (Roche Molecular Biochemicals) and saturating amounts of pLEIN plasmid for 18 h. Fresh medium was replenished at this time. The cells were examined by fluorescence microscopy 48 h after transfection. For selection, the cells were cultured in the presence of 500-2000 mg/ml of G418 (Life Technologies, Grand Island, NY) for 7 days (6).

2.4 Retroviral GFP and RFP Transduction of Tumor Cells (6)

For GFP and RFP gene transduction, 25% confluent cells were incubated with a 1:1 precipitated mixture of retroviral supernatants of PT67 cells and RPMI 1640 (GIBCO) containing 10% FBS (Gemini Biological Products) for 72 h. Fresh medium was replenished at this time. Cells

were harvested by trypsin EDTA 72 h after transduction and subcultured at a ratio of 1:15 into selective medium, which contained 200 mg/ml of G418. The level of G418 was increased stepwise up to 1000 mg/ml. Clones stably expressing GFP or RFP were isolated with cloning cylinders (Bel-Art Products) with the use of trypsin/EDTA and were then amplified and transferred by conventional culture methods.

2.5 Animals (6)

Six-week-old BALB/c *nu/nu* male and female *nude* mice were used. Transgenic C57/B6-GFP mice (35) were obtained from Research Institute for Microbial Diseases, Osaka University, Osaka, Japan. The C57/B6-GFP mice express GFP under the control of the chicken beta-actin promoter and cytomegalovirus enhancer. All of the tissues from this transgenic line, with the exception of erythrocytes and hair, fluoresce green under excitation light. The GFP gene, regulated as described above, was crossed in to nude mice on the C57/B6 background. Both immunocompetent and nude GFP transgenic mice were used.

All animal studies were conducted in accordance with the principles and procedures outlined in the National Institute of Health Guide for the Care and Use of Animals under assurance number A3873-1. Animals were kept in a barrier facility under HEPA filtration. Mice were fed with autoclaved laboratory rodent diet (Tecklad LM-485, Western Research Products, Orange, CA).

2.6 SOI Tumor Models (33)

Tumor fragments (1 mm³), stably expressing GFP or RFP, previously grown s.c. in nude mice, were implanted by SOI on the appropriate organ in nude mice. After proper exposure of the organ to be implanted, 8-0 surgical sutures were used to penetrate the tumor pieces and attach them to the appropriate orthotopic organ. The incision in the skin was closed with a 7-0 surgical suture in one layer. The animals are kept under isoflurane anesthesia during surgery. All procedures of the operation described above were performed with a 37 magnification microscope (MZ6; Leica, Nussloch, Germany).

2.7 Cutaneous Melanoma Model (36)

Six-week-old male C57/B6-GFP mice were injected subcutaneously with 10^6 RFP-expressing mouse B16F0 melanoma cells. Cells were first harvested by trypsinization and washed 3 times with cold serum-containing medium, then kept on ice. Cells were inoculated by intradermal injection of the dorsal skin of the animal in a total volume of 50 μ l within 40 minutes of harvesting.

2.8 Quantitative Analysis of Angiogenesis (6)

Periodically, the tumor-bearing mice were examined by intravital or whole-body fluorescence imaging. The extent of blood vessel development in a tumor was evaluated based on the total length of blood vessels (L) in chosen areas: areas containing the highest number of vessels were identified by scanning the tumors by intravital or whole-body imaging. To compare the level of vascularization during tumor growth, the “hot” areas with the maximum development of vessels per unit area were then quantitated for L expressed in pixels. Captured images were corrected for unevenness in illumination. Then the total number of pixels derived from the blood vessels was quantified with IMAGE PRO PLUS software.

2.9 Skin-Flap Windows (34)

Tumor cells on the various internal organs were visualized through the skull or body wall through different skin-flap windows over the scalp, chest wall, upper abdomen, and lower abdomen. The animals were anesthetized with the ketaminemixture. An arc-shaped incision was made in the skin, and s.c. connective tissue was separated to free the skin flap. The skin flap could be opened repeatedly to image tumor cells on the internal organs through the nearly transparent mouse body walls or skull and simply closed with an 6-0 suture. This procedure greatly reduced the scatter of fluorescent photons.

2.10 Tumor Tissue Sampling (36)

Tumor tissue biopsies were processed from three days to four weeks after inoculation of tumor cells. Fresh tissue were cut into $\sim 1\text{mm}^3$ pieces and pressed on slides for fluorescence microscopy. For analyzing tumor angiogenesis, the tissues were digested with trypsin/EDTA at 37°C for 5 minutes before examination. After trypsinization, tissues were put on pre-cleaned microscope slides (Fisher Scientific, Pittsburgh, PA 15219) and covered with another microscope slide.

ACKNOWLEDGEMENT

These studies were funded in part by National Cancer Institute grant number 1 R43 CA099258-01 and 1 R43 CA103563-01.

REFERENCES

1. Carmeliet, P., 2003, Angiogenesis in health and disease. *Nature Med* 9:653-660.
2. Jain, R.K., 2003, Molecular regulation of vessel maturation. *Nature Med* 9:685-693.
3. Ruoslahti, E., 2002, Specialization of tumour vasculature. *Na Rev Cancer*, 2:83-90.
4. Hendrix, M. J., Sefter, E.A., Hess, A.R., and Sefter, R. E., 2003, Vasculogenic mimicry and tumour-cell plasticity: lessons from melanoma. *Nat Rev Cancer* 3:411-21.
5. McDonald, D.M., and Choyke, P.L., 2003, Imaging of angiogenesis: from microscope to clinic. *Nat Med* 9:713-725.
6. Yang, M., Baranov, E., Li, X-M., Wang, J-W., Jiang, P., Li, L., Moossa, A.R., Penman, S., and Hoffman, R.M., 2001, Whole-body and intravital optical imaging of angiogenesis in orthotopically implanted tumors. *Proc Natl Acad Sci USA*, 98:2616-2621.
7. Auerbach, R., Kubai, L., Knighton, D., and Folkman, J., 1974, A simple procedure for the long-term cultivation of chicken embryos. *Dev Biol* 41:391-394.
8. Crum, R., Szabo, S., and Folkman, J., 1985, A new class of steroids inhibits angiogenesis in the presence of heparin or a heparin fragment. *Science*, 230:1375-1378.
9. Miller, J. W., Stinson, W. G., and Folkman, J., 1993, Regression of experimental iris neovascularization

- with systemic alpha-interferon. *Ophthalmology*, 100:9–14.
10. Passaniti, A., Taylor, R. M., Pili, R., Guo, Y., Long, P. V., Haney, J. A., Pauly, R. R., Grant, D. S., and Martin, G. R., 1992, A simple, quantitative method for assessing angiogenesis and antiangiogenic agents using reconstituted basement membrane, heparin, and fibroblast growth factor. *Lab Invest*, 67:519–528.
 11. Alessandri, G., Raju, F., and Gullino, P. M., 1983, Mobilization of capillary endothelium in vitro induced by effectors of angiogenesis in vivo. *Cancer Res*, 43:1790–1797.
 12. Deutsch, T. A., and Hughes, W. F., 1979, Suppressive effects of indomethacin on thermally induced neovascularization of rabbit corneas. *Am J Ophthalmol*, 87:536–540.
 13. Korey, M., Peyman, G. A., and Berkowitz, R., 1977, The effect of hypertonic ointments on corneal alkali burns. *Ann Ophthalmol*, 9:1383–1387.
 14. Mahoney, J. M., and Waterbury, L. D., 1985, Drug effects on the neovascularization response to silver nitrate cauterization of the rat cornea. *Curr Eye Res*, 4:531–535.
 15. Li, W. W., Grayson, G., Folkman, J., and D'Amore, P. A., 1991, Sustained-release endotoxin. A model for inducing corneal neovascularization. *Invest. Ophthalmol Vis Sci*, 32:2906–2911.
 16. Epstein, R. J., Hendricks, R. L., and Stulting, R. D., 1990, Interleukin-2 induces corneal neovascularization in A/J mice. *Cornea*, 9:318–323.
 17. Gimbrone, M. A., Cotran, I. S., Leapman, S. B., and Folkman, J., 1974, Tumor growth and neovascularization: an experimental model using the rabbit cornea. *J Natl Cancer Inst*, 52:413–427.
 18. Fournier, G. A., Luty, G. A., Watt, S., Fenselau, A., and Patz, A., 1981, A corneal micropocket assay for angiogenesis in the rat eye. *Invest Ophthalmol Vis Sci*, 21:351–354.
 19. Muthukkaruppan, V., and Auerbach, R., 1979, Angiogenesis in the mouse cornea. *Science*, 205:1416–1418.
 20. Papenfuss, H. D., Gross, J. F., Intaglietta, M., and Treese, F. A., 1979, A transparent access chamber for the rat dorsal skin fold. *Microvasc Res* 18:311–318.
 21. Gross, J., Roemer, R., Dewhirst, M., and Meyer, T., 1982, *Int J Heat Mass Transfer*, 25:1313–1320.
 22. Dewhirst, M., Gross, J., Sim, D., Arnold, P., and Boyer, D., 1984, The effect of rate of heating or cooling prior to heating on tumor and normal tissue microcirculatory blood flow. *Biorheology*, 21:539–558.
 23. Fukumura, D., Xavier, R., Sugiura, T., Chen, Y., Park, E. C., Lu, N., Selig, M., Nielsen, G., Taksir, T., Jain, R. K., et al., 1998, Tumor induction of VEGF promoter activity in stromal cells. *Cell*, 94:715–725.
 24. Li, C. Y., Shan, S., Huang, Q., Braun, R. D., Lanzen, J., Hu, K., Lin, P., and Dewhirst, M. W., 2000, Initial stages of tumor cell-induced angiogenesis: evaluation via skin window chambers in rodent models. *J Natl Cancer Inst*, 92:143–147.
 25. Al-Mehdi, A. B., Tozawa, K., Fisher, A. B., Shientag, L., Lee, A., and Muschel, R. J., 2000, Intravascular origin of metastasis from the proliferation of endothelium-attached tumor cells: a new model for metastasis. *Nat Med*, 6:100–102.
 26. Huang, Q., Shan, S., Braun, R. D., Lanzen, J., Anyrhambatla, G., Kong, G., Borelli, M., Corry, P., Dewhirst, M. W., and Li, C. Y., 1999, Noninvasive visualization of tumors in rodent dorsal skin window chambers. *Nat Biotechnol*, 17:1033–1035.
 27. Cowen, S. E., Bibby, M. C., and Double, J. A., 1995, Characterisation of the vasculature within a murine adenocarcinoma growing in different sites to evaluate the potential of vascular therapies. *Acta Oncol*, 34:357–360.
 28. Hoffman, R.M., 2002, Green fluorescent protein imaging of tumour growth, metastasis, and angiogenesis in mouse models. *Lancet Oncology*, 3:546–556.
 29. O' Reilly, M. S., Boehm, T., Shing, Y., Fukai, N., Vasios, G., Lane, W. S., Flynn, E., Birkhead, J. R., Olsen, B. R., and Folkman, J., 1997, Endostatin: an endogenous inhibitor of angiogenesis and tumor growth. *Cell*, 88, 277–285.
 30. Drevs, J., Hofmann, I., Hugenschmidt, H., Wittig, C., Madjar, H., Muller, W., Wood, J., Martiny-Baron, G., Unger, C., and Marme, D., 2000, Effects of PTK787/ZK 222584, a specific inhibitor of vascular endothelial growth factor receptor tyrosine kinases, on primary tumor, metastasis, vessel density, and blood flow in a murine renal cell carcinoma model. *Cancer Res*, 60:4819–4824.
 31. Prewett, M., Huber, J., Li, Y., Santiago, A., O'Connor, W., King, K., Overholser, J., Hooper, A., Pytowski, B., Witte, L., et al., 1999, Antivascular endothelial growth factor receptor (fetal liver kinase 1) monoclonal antibody inhibits tumor angiogenesis and growth of several mouse and human tumors. *Cancer Res*, 59:5209–5218.
 32. Kurebayashi, J., Kunisue, H., Yamamoto, S., Kurosumi, M., Otsuki, T., and Sonoo, H., 2000, Paradoxical hormone responses of KPL-1 breast cancer cells in vivo: a significant role of angiogenesis in tumor growth. *Oncology*, 59:158–165.
 33. Hoffman, R.M., 1999, Orthotopic metastatic mouse models for anticancer drug discovery and evaluation: a bridge to the clinic. *Investigational New Drugs* 17:343–359.
 34. Yang, M., Baranov, E., Wang, J-W., Jiang, P., Wang, X., Sun, F-X., Bouvet, M., Moossa, A.R., Penman, S., and Hoffman, R.M., 2002, Direct external imaging of nascent cancer, tumor progression, angiogenesis, and metastasis on internal organs in the

- fluorescent orthotopic model. *Proc Natl Acad Sci USA* 99:3824-3829.
35. Okabe, M., Ikawa, M., Kominami, K., Nakanishi, T., and Nishimune, T., 1997, 'Green mice' as a source of ubiquitous green cells. *FEBS Letters*, 407: 313-319.
 36. Yang, M., Li, L., Jiang, P., Moossa, A.R., Penman, S., and Hoffman, R.M., 2003, Dual-color fluorescence imaging distinguishes tumor cells from induced host angiogenic vessels and stromal cells. *Proc Natl Acad Sci USA*, 100:14259-14262.
 37. Levenson, R., Yang, M., and Hoffman, R.M., 2004, Whole-body dual-color differential fluorescence imaging of tumor angiogenesis enhanced by spectral unmixing. *Proc Am Assoc Cancer Res*, accepted abstract.
 38. Yamamoto, N., Yang, M., Jiang, P., Xu, M., Tsuchiya, H., Tomita, K., Moossa, A.R., and Hoffman, R.M., 2003, Determination of clonality of metastasis by cell-specific color-coded fluorescent-protein imaging. *Cancer Res*, 63:7785-7790.